

The John Charnley Award

An Accurate and Extremely Sensitive Method to Separate, Display, and Characterize Wear Debris

Part 2: Metal and Ceramic Particles

Fabrizio Billi PhD, Paul Benya PhD,
Aaron Kavanaugh BS, John Adams MD, PhD,
Harry McKellop PhD, Edward Ebramzadeh PhD

Published online: 20 September 2011
© The Association of Bone and Joint Surgeons® 2011

Abstract

Background Metal-on-metal and ceramic-on-ceramic bearings were introduced as alternatives to conventional polyethylene in hip arthroplasties to reduce wear. Characterization of wear particles has been particularly challenging due to the low amount and small size of wear particles. Current methods of analysis of such particles have shortcomings, including particle loss, clumping, and inaccurate morphologic and chemical characterization.

Questions/purposes We describe a method to recover and characterize metal and ceramic particles that (1) improves

One or more of the authors has received funding from NIH/NIAMS (FB, PB, JA), Medtronic Sofamor Danek, Inc (Minneapolis, MN, USA) (FB, EE), Wright Medical Technology, Inc (Arlington, TN, USA) (FB), DePuy Orthopaedics, Inc (Warsaw, IN, USA) (FB, HM), Stryker Orthopaedics (Mahwah, NJ, USA) (FB), and Biomet, Inc (Warsaw, IN, USA) (FB). One or more of the authors (HM) has received royalties from DePuy.

Each author certifies that his or her institution approved or waived approval for the reporting of this investigation and that all investigations were conducted in conformity with ethical principles of research.

This is a companion article to Billi F, Benya P, Kavanaugh A, Adams J, McKellop H, Ebramzadeh E. The John Charnley Award. An Accurate and Sensitive Method to Separate, Display, and Characterize Wear Debris. Part 1: Polyethylene Particles. *Clin Orthop Relat Res.* 2011. doi: [10.1007/s11999-011-2057-x](https://doi.org/10.1007/s11999-011-2057-x)

Electronic supplementary material The online version of this article (doi:[10.1007/s11999-011-2058-9](https://doi.org/10.1007/s11999-011-2058-9)) contains supplementary material, which is available to authorized users.

F. Billi (✉), P. Benya, A. Kavanaugh, J. Adams,
H. McKellop, E. Ebramzadeh
Department of Orthopaedic Surgery, The J. Vernon Luck Sr.,
M.D., Orthopaedic Research Center at Orthopaedic Hospital,
UCLA/Orthopaedic Hospital, David Geffen School of Medicine,
Los Angeles, CA 90007, USA
e-mail: fbilli@laoh.ucla.edu

particle purification, separation, and display; (2) allows for precise particle shape characterization; (3) allows accurate chemical identification; and (4) minimizes particle loss.

Methods After enzymatic digestion, a single pass of ultracentrifugation cleaned and deposited particles onto silicon wafers or grids for imaging analysis. During centrifugation, particles were passed through multiple layers of denaturants and a metal-selective high-density layer that minimized protein and nucleic acid contamination. The protocol prevented aggregation, providing well-dispersed particles for chemical and morphologic analysis. We evaluated the efficacy and accuracy of this protocol by recovering gold nanobeads and metal and ceramic particles from joint simulator wear tests.

Results The new protocol recovered particles ranging in size from nanometers to micrometers and enabled accurate morphologic and chemical characterization of individual particles.

Conclusion Both polyethylene and metal wear debris can be simultaneously analyzed from the same sample by combining a silicon wafer display protocol for polyethylene and the metal and ceramics silicon wafer display protocol.

Clinical Relevance Accurate analysis of wear debris is essential in understanding the processes that produce debris and a key step in development of more durable and bio-compatible implants.

Introduction

Central to the success of orthopaedic implants is their longevity and their capacity to benefit a patient's mobility while relieving pain and preventing its recurrence. Although many elements of implant design and materials play a role, the effects of wear in the bearing couple and consequent

production of wear particles and ions have a large influence on long-term survival and the chance of revision surgery.

In the last decade, metal-on-metal (MOM) hip arthroplasties have gained increased popularity because they produce lower volumetric wear and the sockets are stronger than the relatively thinner polyethylene liners with large-diameter metal-on-polyethylene joint arthroplasties [1, 13, 16, 21, 39]. However, an increasing number of investigators report serious complications associated with MOM implants, including adverse soft-tissue reactions, bursae, metallosis, osteolysis, squeaking, and pain [6, 14, 19, 23, 26–28, 33, 34, 40]. There also are concerns regarding elevated metal ion content, toxicity, and their associated effects [7, 18, 22, 37].

While both particulate debris and metal ions are likely etiologic agents in adverse events such as pseudotumors or hypersensitivity, it is unclear whether local reactions are predominantly caused by intracellular corrosion of wear particles or systemic ions. To understand such relationships, the process of isolating wear particles must maintain their *in vivo* morphologic distribution and chemical composition.

Our research group has previously reported techniques to isolate metal wear particles released from MOM THAs [8, 9, 12, 16, 17]. These and other studies [3, 4, 10, 15, 16, 24, 36, 38, 41] use complex techniques because metal wear particles are nanometer sized and not chemically inert (Table 1). In general, metal wear particles are known to be mainly composed of chromium oxide (CrOx) and cobalt-chrome (CoCr). However, these analyses have shortcomings, including particle loss, clumping, and inaccurate morphologic and chemical characterization, among others.

We designed a method to provide a simple, two-step approach for particle isolation and purification. We developed the new protocol with the aim to purify, recover, and analyze wear debris from any material having a density of greater than 2.0 g/mL. We refer to the protocol as the silicon wafer display (SWD) method since a key advantage is that the particles are collected on a featureless wafer for display without the use of filtration. We refer to the specific SWD protocol for metal and ceramic particles as MC-SWD. The protocol was intended to (1) improve particle purification, separation, and display; (2) allow accurate chemical identification; (3) allow precise particle shape characterization; and (4) minimize particle loss. We evaluated the efficacy and accuracy of this protocol by recovering gold nanobeads and metal and ceramic particles from joint simulator wear tests.

Materials and Methods

The experimental procedure requires a number of steps (Fig. 1). All solutions employed for particle isolation were

filtered through 0.02- μm Anodisc™ filters (47 mm in diameter; Whatman International Ltd, Maidstone, UK).

Metal and ceramic particles were produced during wear tests of CoCr alloy and alumina bearings. The bearing couples were tested in hip and spine simulators, according to previously reported protocols [29]. A total of three MOM and three metal-on-ceramic (MOC) hip implants were tested in a six-station orbital hip simulator (Shore Western Manufacturing Inc, Monrovia, CA), applying a double-peak curve load profile [35] (maximum, 2000 N). Three MOM spine implants were tested in a custom-made, three-station spine biaxial wear simulator and load and motion profiles were based on the ISO/DIS 18192-1 standard [25]. All wear lubricants consisted of 90% bovine serum (protein concentration, 63 g/L), 0.2% sodium azide (NaN_3), 20 mmol/L ethylenediaminetetraacetic acid (EDTA), pH 7.3 [32]. Since proteases, cellulases, and other carbohydrate-degrading enzymes could not completely remove insoluble material derived from bacteria, fungus, or mold, NaN_3 was essential to prevent such contamination. Lubricant samples were stored at -20°C or -80°C until analysis.

MOM and MOC samples from the hip wear simulator and MOM samples from the spine wear simulator in the interval 0- to 0.25-million cycles were rotated end-over-end at 28 rpm for 24 hours at room temperature to evenly disperse the particles in the lubricant. Each sample was then treated according to an optimized proteolytic digestion protocol (Fig. 2) to avoid particle degradation caused by more aggressive digestion protocols, such as bases and acids [10, 11]. The protocol is reported in detail in Appendix 1 (supplemental materials are available with the online version of CORR). Briefly, since properly functioning implants exhibited low wear, a centrifugation step preceded protein digestion to concentrate the metal wear debris. The pellet was subsequently digested with proteinase K. The particles were then purified via density gradient centrifugation through multiple layers of denaturants and a metal-selective high-density layer that minimized protein and nucleic acid contamination and displayed the particles on a 5- × 5-mm featureless display silicon wafer (Ted Pella, Inc, Redding, CA, USA) coated with a monolayer of marine mussel glue (Cell-Tak™; BD Biosciences, San Jose, CA, USA).

Each wafer was glued to an aluminum stub and coated with 10 Å iridium (EBS; SouthBay Technology, San Clemente, CA) before imaging with a field emission scanning electron microscope (FE-SEM) (Supra VP-40; Zeiss, Peabody, MA) at a voltage of 15 kV. Transmission electron microscopy (TEM) grids were imaged within the FE-SEM using a scanning transmission electron microscopy (STEM) detector at an acceleration voltage of 25 kV. At least three different fields of view at three different locations on the wafer or grid were imaged. This maximized counting and

Table 1. Digestion protocols to isolate metal wear debris

| Study | Year | Digestion | Purification | Display | Image | Total number of particles examined | Measured parameters | Statistics |
|-------------------------|------|-----------------------------------------------------|--------------------------------------------------------------------------------------|-----------------------------|------------|------------------------------------|------------------------------------------------------------------------------------------------------|---------------------|
| Schmiedberg et al. [38] | 1994 | Papain, proteinase K (NaOH wash) | Multiple sequential WCS (7 steps) | Drop evaporation | SEM | 20 | Length, width | Mean, SD |
| Doorn et al. [16]* | 1998 | Papain, proteinase K | Multiple sequential WCS (4 steps) | Nebulization on TEM grid | TEM | 1–580 | Diameter | Box plots |
| Tipper et al. [41] | 1999 | KOH 60°C | Extraction with chloroform:methanol (2:1) and repeated washes with 50% (v/v) acetone | Filtration | SEM | 100 | Mean d_{max} , aspect ratio (length/width), area, perimeter | One-way ANOVA |
| Catelas et al. [10] | 2001 | Papain, proteinase K | Multiple sequential WCS (6 steps) | Resin embedding and slicing | TEM | 700–1300 | Length, width | One-way ANOVA |
| Brown et al. [4] | 2007 | Papain, proteinase K, yeast lytic enzyme, Zymolase® | Multiple sequential WCS (12 steps) | Sequential filtration | SEM | 150 | d_{max} | One-way ANOVA |
| Billi et al. | 2011 | Proteinase K, 37°C | Density gradient centrifugation (1 step) | Silicon wafer or TEM grid | SEM or TEM | Minimum 1000 | d_{min} , d_{max} , P, A, ECD, FL, FB, FF, AR, E, R, shape and chemical composition distribution | Nonparametric tests |

* Particles isolated from tissue samples; WCS = washing/centrifugation/supernatant removal; TEM = transmission electron microscopy; SEM = scanning electron microscopy; d_{min} = minimum Feret's diameter; d_{max} = maximum Feret's diameter; P = perimeter; A = area; ECD = equivalent circle diameter; FL = fiber length; FB = fiber breadth; FF = form factor; AR = aspect ratio; E = elongation; R = roundness.

Fig. 1 A flowchart illustrates an outline of the experiment.

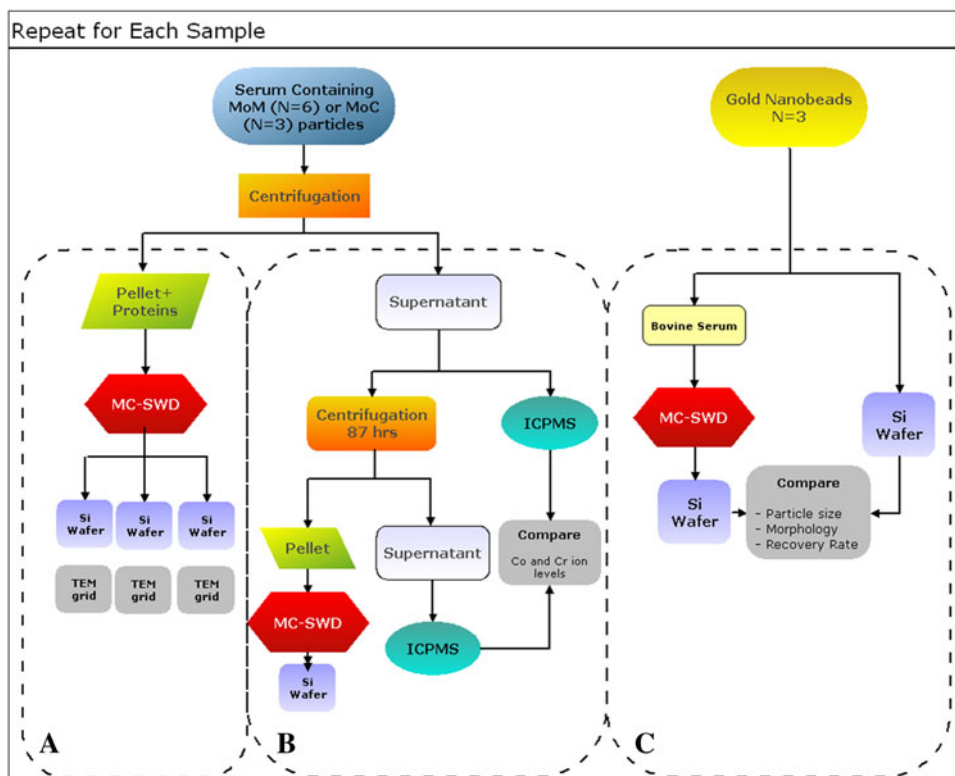
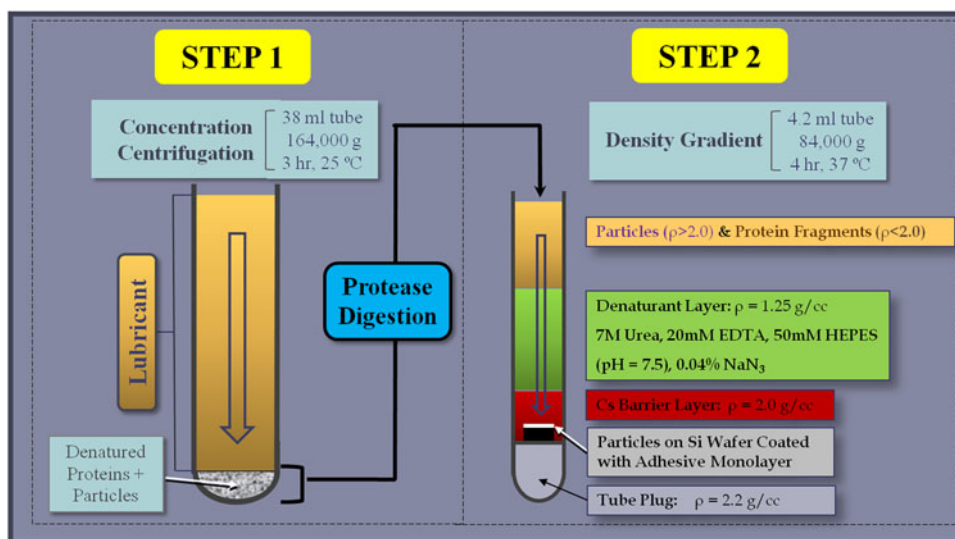


Fig. 2 A schematic diagram outlines the MC-SWD protocol.



discrimination of nanometer-sized particles and yielded data from 300 to 2100 particles per sample. STEM was used to gather information about the phase distribution within particles.

Morphologic characterization was performed according to the protocol detailed in the Appendix 1. Briefly, we outlined the particles on each micrograph using digital image processing software (MetaMorph™ 6.3r7; Molecular Devices Corp, Sunnyvale, CA, USA) and an automated routine. Size and morphologic descriptors were calculated according to ASTM F1877-05 [2]. The shapes of the

particles were quantified using a custom-defined algorithm, also detailed in Appendix 1.

We calculated the area of the particles using the image analysis software and calculated the total number of particles generated per cycle in the wear simulator by taking into account the cross-sectional area of the centrifuge tube, the dilutions of the MC-SWD protocol, and the total number of wear cycles. Chemical composition, as determined by x-ray energy dispersive analysis (EDS) (NORAN™ System Six; Thermo Fisher Scientific Inc, Waltham, MA, USA), was used to further discriminate between the particles. Each

particle was classified according to its shape, size, and chemical composition. Initially, statistical analysis was performed on a sample to evaluate the distribution of the particles on the wafer and establish the minimum number of particles needed to assure the distribution was well represented. First, descriptive measures, including median, skewness, and kurtosis were calculated. As expected, the distributions were not normal for any of the parameters. The distributions were graphed using frequency counts and distribution bar plots. The particle distributions were compared between two samples using the Kolmogorov-Smirnov Z test (SPSS[®] Version 14; IBM Corp, Somers, NY, USA). P-P plots were constructed for each parameter and were used to compare the distribution among different images within the sample and among different samples.

The effectiveness and accuracy of the protocol were evaluated using highly purified gold nanobeads with well-defined shapes and size distribution. Specifically, 350 μL of gold

nanoparticles (49.6 $\mu\text{g}/\text{mL}$; Nanopartz Inc, Loveland, CO, USA), having a mean ($\pm\text{SD}$) diameter of 50 ± 2 nm, was mixed with bovine serum (protein concentration, 60 mg/mL; HyClone, Logan, UT, USA) to a final volume of 36 mL. The serum was then digested according to the MC-SWD protocol. As a control, 50 μL of the gold nanoparticles was added to 1.15 mL ultrapure water in a SW60 polyallomer tube (Beckman Coulter, Inc, Brea, CA, USA) and ultracentrifuged for 30 minutes at 3368 g and 4 hours at 84,000 g without digestion onto a silicon wafer before characterization. Differences between the gold nanobeads in digested serum and the control were calculated using Student's t test.

To evaluate particle loss, an aliquot of supernatant collected after the concentrating centrifugation step of a MOM hip sample was analyzed via inductively coupled plasma mass spectrometry (ICPMS) for Cr and Co ion content. Other aliquots were transferred into six SW60 tubes and centrifuged for another 87 hours at 485,000 g. After this time, the supernatant in each tube was transparent and was removed and saved, except for the last 0.4 mL. Those small portions were pooled and submitted to the complete digestion and display of the MC-SWD protocol. An aliquot of saved supernatant was analyzed via ICPMS for Co and Cr.

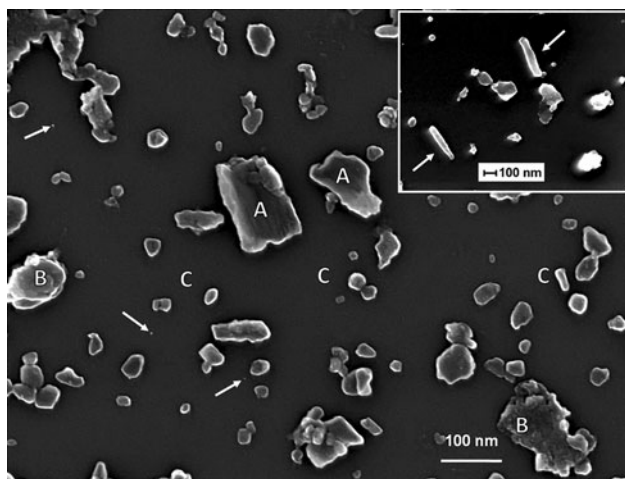


Fig. 3 FE-SEM images show MOM hip particles collected on a silicon wafer, demonstrating the even distribution of particles on the wafer. As a general rule, the biggest and smoother particles contain Co (A) whereas the large particles (B) and the majority of the smaller particles (C) with a rougher surface contain CrOx. The smallest particles (white arrows) were less than 5 nm in size. The inset shows an example of rod-shaped particles (white arrows); note difference in magnification.

Results

Particles displayed on silicon wafers were well separated with few agglomerates (Fig. 3). Detailed chemical characterization was possible on particles as small as 12 nm (Fig. 4), allowing detailed classification based on both morphologic characteristics and chemical composition. The distributions of the particles were similar at different locations on the wafer (Fig. 5). Power analysis indicated, with an alpha of 0.05 and a power of 80%, 900 particles per sample were sufficient to detect differences of 0.02 μm in maximum Feret's diameter (d_{max}), 9% in Co concentration, and 6% in Cr concentration, and differences of 5%, 1.5%, 0.1%, and 3% of round, oval, irregular-, and rod-shaped particles, respectively.

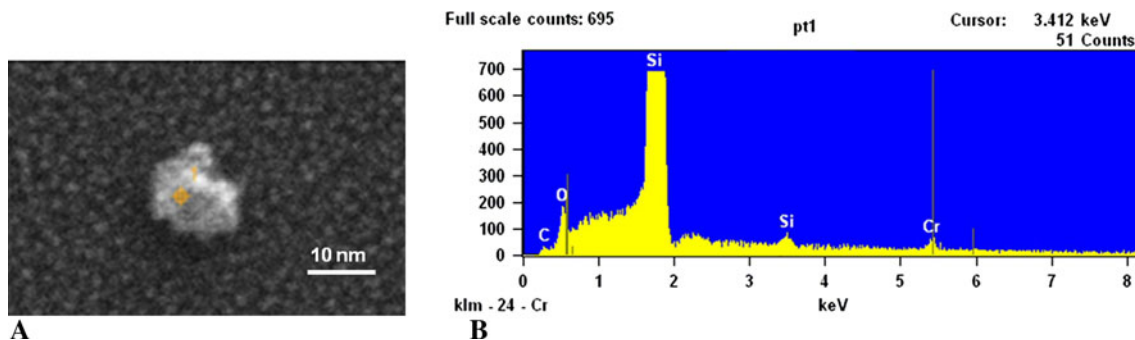


Fig. 4A–B (A) A 12-nm CrOx particle from a MOM hip sample is shown. (B) The EDS spectrum of this particle is shown.

Fig. 5A–B Graphs show a comparison of P-P plots for d_{\max} from two different areas on a wafer (**A** and **B**), confirming the uniform distribution of particles. Cum Prob = cumulative probability.

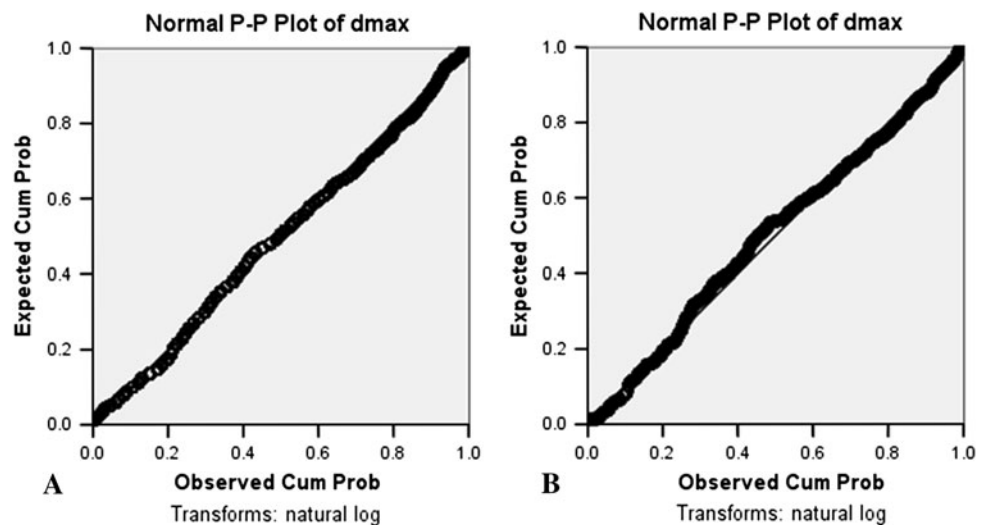


Table 2. Comparison of elemental composition for particles from metal-on-metal hip and spine joint simulators.

| Joint | CrOx | | Co | | Other |
|---------------|--------|------------|--------|------------|-------|
| | % | d_{\max} | % | d_{\max} | |
| Hip (n = 9) | 83 ± 7 | 0.1 ± 0.08 | 11 ± 3 | 0.3 ± 0.2 | 6 ± 4 |
| Spine (n = 9) | 67 ± 9 | 0.14 ± 0.1 | 27 ± 7 | 0.5 ± 0.3 | 6 ± 4 |

Values are expressed as mean ± SD; CrOx = chromium oxide; Co = cobalt; d_{\max} = maximum Feret's diameter (microns).

The vast majority of the particles from MOM hip simulator samples were mostly round and oval CrOx particles (Table 2). A small percentage of Co-rich particles had irregular or rodlike shapes, smooth surface textures, and larger sizes than the CrOx particles (Fig. 3). Also, a small percentage of particles was identified as iron chromium (FeCr) (likely due to fretting of the wear simulator's stainless-steel fixtures) and considered to be a contaminant. TEM analysis showed the CrOx particles were largely amorphous (light gray) whereas Co-rich particles were mostly crystalline (dark gray) (Fig. 6). In contrast, a higher percentage of particles isolated from spine simulator lubricant contained Co, whereas the percentage of CrOx particles was smaller (Table 2). MOC hip samples contained fewer particles than MOM hip samples. To obtain a sufficient number of particles on the wafer, we increased the concentration of the sample threefold. However, the particles of interest, that is, those due to wear of the bearing surfaces and thus containing Al, Cr, or Co, were less than 60% of the total number of particles observed (Fig. 7). The remaining particles contained mainly FeCr and titanium oxide (TiOx) and were considered contaminants due to hip simulator fixture wear. The average d_{\max} (Appendix 1) of the particles of interest was $0.15 \pm 0.12 \mu\text{m}$. The majority of the particles of interest contained Al, whereas Co-rich particles were more frequent than CrOx particles (Fig. 7).

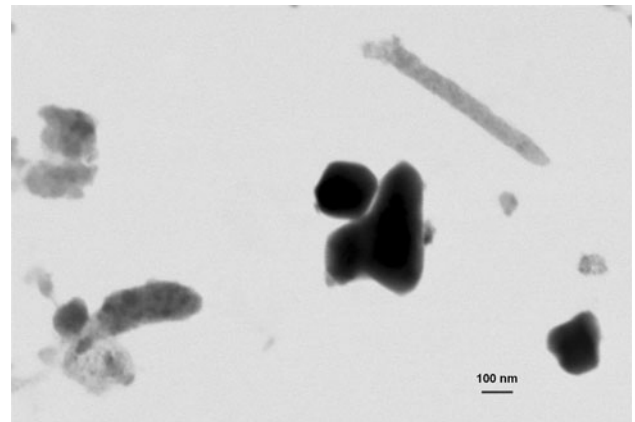
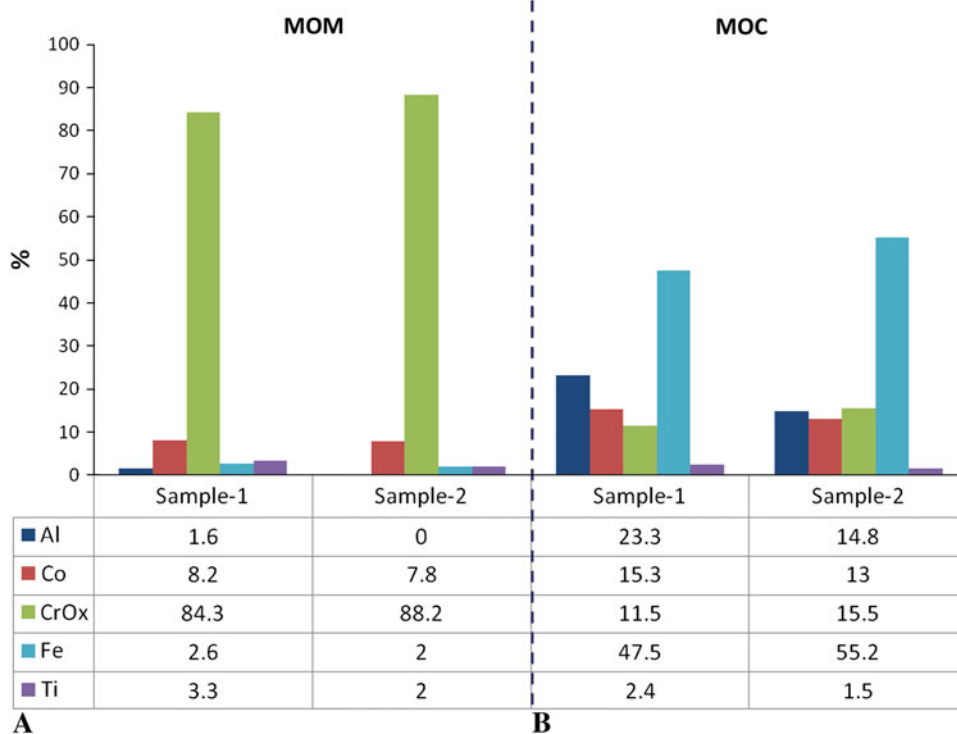


Fig. 6 An image shows metal particles on a TEM grid (STEM detector). Amorphous CrOx particles are light gray and crystalline Co-rich particles are dark gray. Predominantly amorphous or crystalline particles are easily recognized, as well as subregions that are more or less crystalline inside a single particle. Furthermore, access to a monolayer of particles assures the image is not the result of superimposed particles.

We assessed the validity of the MC-SWD protocol for particle recovery using standardized gold nanobeads collected directly by centrifugation onto a wafer or mixed with serum and processed by the entire MC-SWD protocol. We recovered $92\% \pm 5\%$ of the nanobeads processed through the MC-SWD protocol.

Particle loss evaluation showed Co level in the supernatant before the 87-hour centrifugation was $37.5 \pm 1.5 \text{ ppm}$; after centrifugation, it was $37.3 \pm 1.6 \text{ ppm}$ ($p = 0.03$); Cr level was $14.9 \pm 0.8 \text{ ppm}$ before centrifugation; after centrifugation, it was $14.5 \pm 0.7 \text{ ppm}$ ($p = 0.05$). Thus, no particles remained in the original concentrating supernatant by depletion analysis. In addition, when the 87-hour supernatant was processed according to the MC-SWD protocol, few particles were identified on the wafer, confirming the high percentage of recovery of the standard MC-SWD protocol.

Fig. 7A–B Graphs show the chemical distribution of the particles for (A) MOM and (B) MOC samples.



Discussion

MOM and ceramic-on-ceramic bearings were introduced as alternatives to conventional polyethylene in hip arthroplasties to reduce wear. Characterization of wear particles has been particularly challenging due to the low amount and small size of wear particles. Current methods of analysis of such particles have shortcomings, including particle loss, clumping, and inaccurate morphologic and chemical characterization. We described a two-step particle isolation and characterization protocol designed to (1) minimize particle loss; (2) improve particle purification, separation, and display; (3) allow accurate chemical identification; and (4) allow precise particle shape characterization. We evaluated the efficacy and accuracy of this protocol by recovering gold nanobeads and metal and ceramic particles from joint simulator wear tests.

One limitation of the current protocol is that it cannot overcome contamination due to microbial growth during wear testing. However, since NaN_3 is normally added to many simulator tests, microbial growth is usually prevented. A second limitation of the study is that gold nanobeads used to assess recovery rate are imperfect surrogates for metal wear particles; they are 50 nm in diameter and reflect the average size of many MOM wear particles and are spherical and thus comparable to the particles characterized as “round.” However, spherical shape presents the smallest

ratio of particle surface area to the wafer surface; thus, the 92% recovery rate of gold beads may be an underestimate of the recovery of the more irregularly shaped wear particles. On the other hand, it is possible round, high-density (19.3 g/mL) gold nanobeads interact differently with proteins and lipids compared to irregular CoCr particles.

Decreased handling and multifunctional centrifugation greatly reduced particle loss. Particle concentration occurred before digestion. The undigested proteins, acting as a cushion, prevented possible artifactual particle aggregation due to centrifugal force. Subsequently, complete protein digestion occurred under conditions of maximal protein denaturation (8 mol/L urea) and stabilization of proteinase K by calcium against autolysis. The proteins were digested in the original tube used to collect the particles, and only the particle suspension was transferred to the purification/display gradient. Purification and display were simultaneously accomplished in a single centrifugation whereas in previous protocols this has been done in multiple washing/centrifugation steps (Table 3), followed by removal of the supernatant and/or transfer to a second tube (Table 1) [10, 16, 38, 41]. Additionally, in the MC-SWD protocol, biologic contaminants (densities < 2.0 g/mL) could not pass into the cesium trifluoroacetate layer and only wear particles reached the wafer whereas in other protocols filters could collect biologic contaminants. The purity and minimum agglomeration of the particles are apparent in the FE-SEM images (Fig. 3).

The wafer provided a high-contrast, virtually featureless surface for deposition. Other investigators have characterized metal particles that were apparently either

agglomerated, too close, or stacked on top of each other [4, 10, 20, 30, 31, 41]. As a result, the spectrum obtained via EDS analysis may have combined signals from multiple particles with different chemical compositions. In the MC-SWD protocol, particle separation allowed for precise chemical characterization. With the FE-SEM used in our study, we were able to successfully characterize particles as small as 12 nm (Fig. 4). The ability to display well-dispersed particles is also possible with TEM grids.

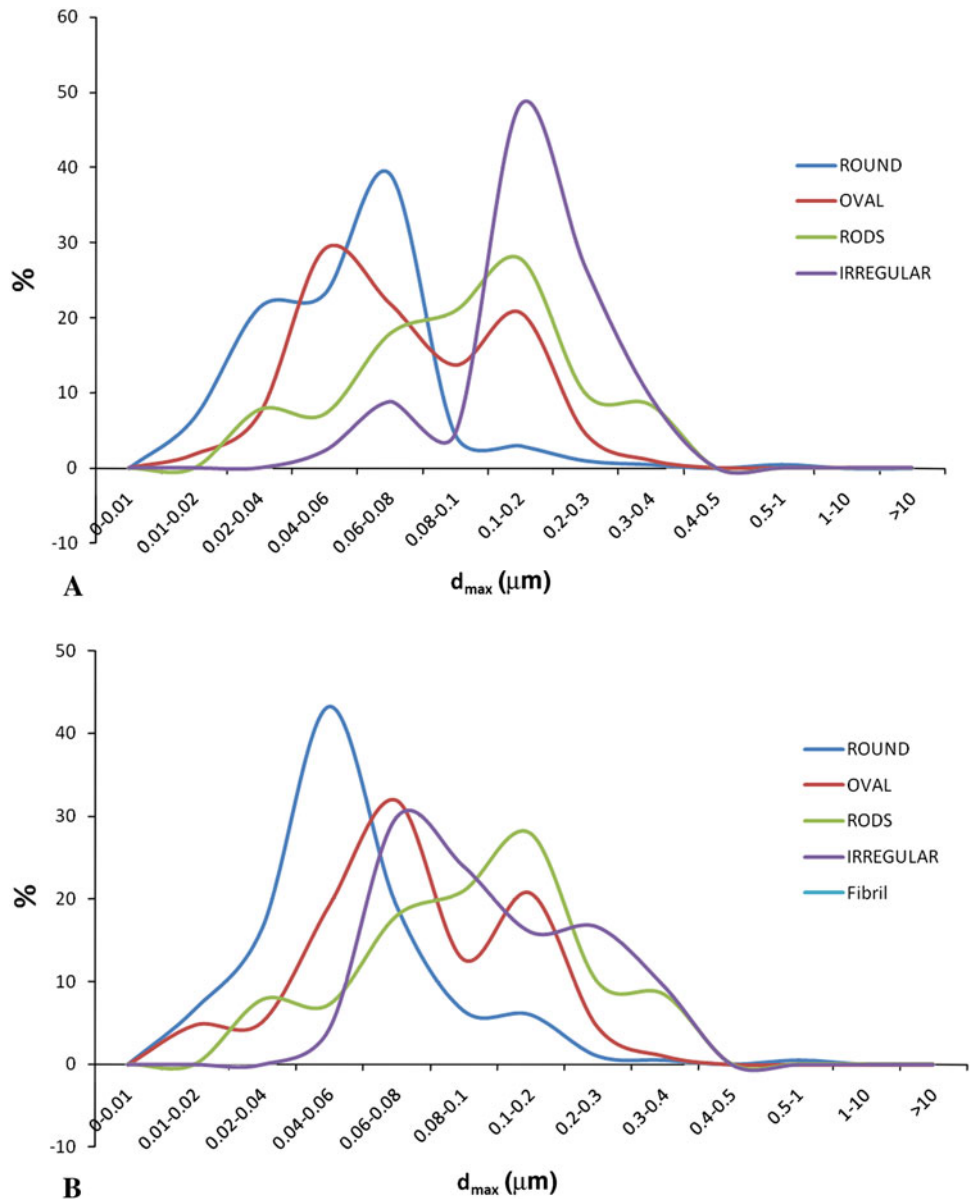
As wear rates have declined in modern MOM and MOC bearings, the ability to identify contaminant particles has become critical since their percentage may increase. The size distribution can be skewed by not taking into account the contaminants (Fig. 8A) or removing them from the calculation (Fig. 8B). In some samples from apparently

Table 3. Steps involved in particle isolation protocols

| Steps | Schmiedberg et al. [38] | Doorn et al. [16] | Catelas et al. [10] | Brown et al. [4] | Billi et al. |
|-----------|-------------------------|-------------------|---------------------|------------------|--------------|
| WCS | 7 | 4 | 6 | 12 | |
| Dilution | 2 | 4 | 3 | 8 | 1 |
| Digestion | 2 | 2 | 2 | 12 | 1 |
| Boiling | | 4 | 3 | 5 | |
| Heating | | | | 1 | |

WCS = washing/centrifugation/supernatant removal.

Fig. 8A–B Graphs show, for MOC low-wear samples, precise chemical characterization and discrimination are critical to avoid skewed distributions as shown in MOC samples (A) with and (B) without contaminants.



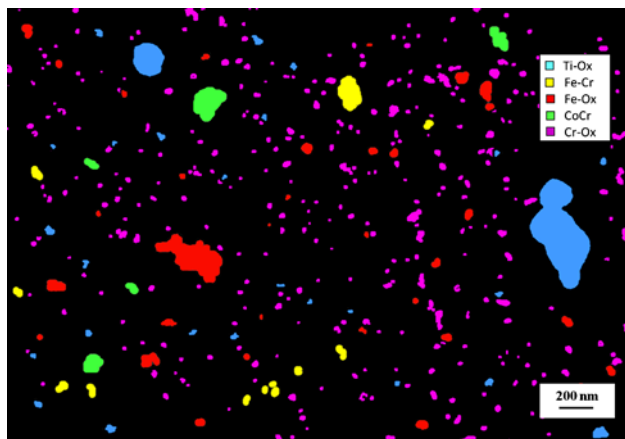
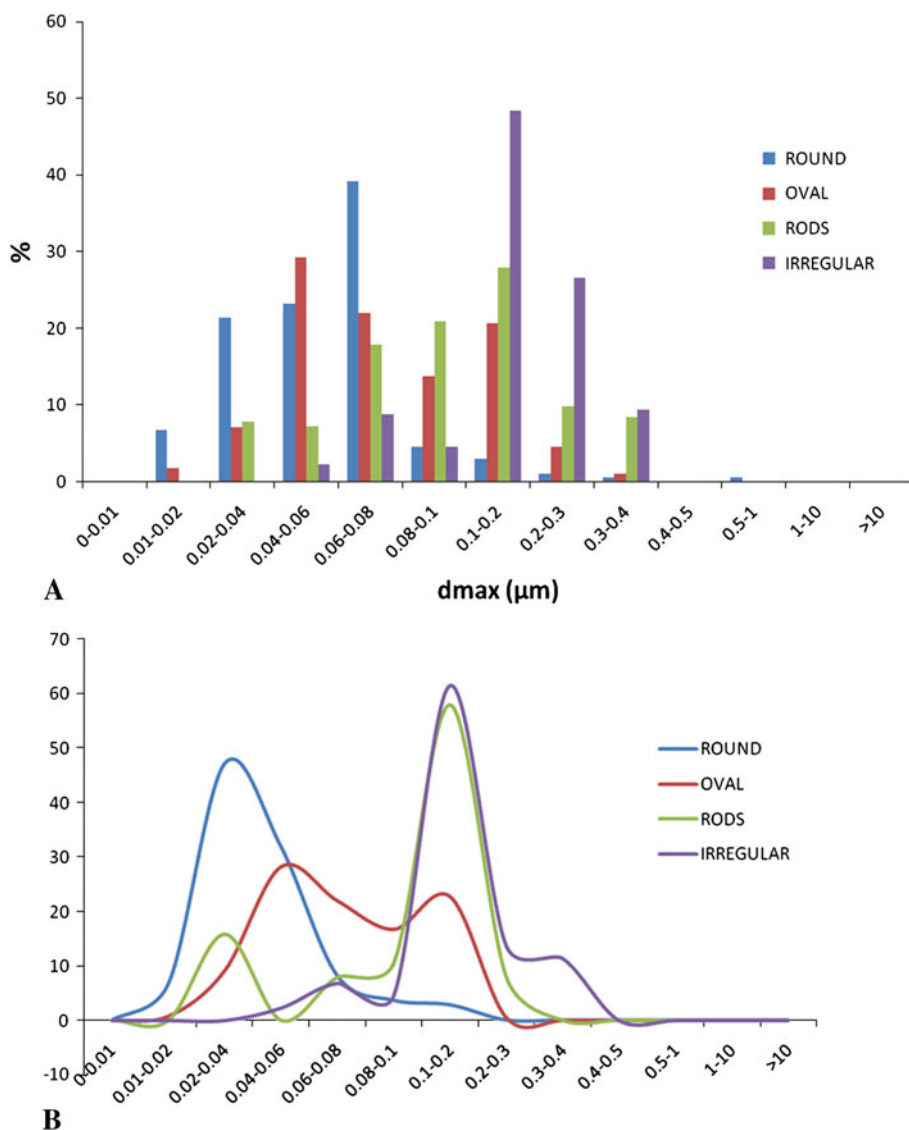


Fig. 9 An image shows chemical characterization of particles on a wafer for a MOC hip sample. Due to the extremely low wear of the ceramic counterface, no particles containing Al were detected in this field.

well-functioning wear simulators, contaminants can actually overwhelm wear particles (Fig. 9). This highlights the importance of even distribution and separation of particles with the SWD method, allowing accurate chemical characterization. In contrast, laser-based particle analysis tools cannot distinguish composition based on refractive index since the particles generally do not have spherical geometry. Furthermore, if the particles are spread over a wide size range (from few nanometers to several tens of micrometers), results from laser diffraction techniques may be skewed toward the larger particles. Finally, laser-based techniques cannot discriminate between particles that have similar sizes (eg, 40 and 60 nm will blend into a 50-nm band).

Although a few descriptors are sufficient to establish size distribution, morphologic characterization should accurately describe shapes, typically requiring more than

Fig. 10A–B Graphs show shape distribution as a function of maximum Feret’s diameter (d_{max}) for a typical MOM sample. Particle shapes were automatically extracted via a dedicated algorithm and could be associated to any other parameter. (A) A distribution of d_{max} for various shapes is shown. (B) Peaks in the distribution of particles with various shapes are more readily identified in this line graph; round particles are usually the smallest particles whereas irregular particles are larger; oval particles and rods are more dispersed across the entire spectrum.



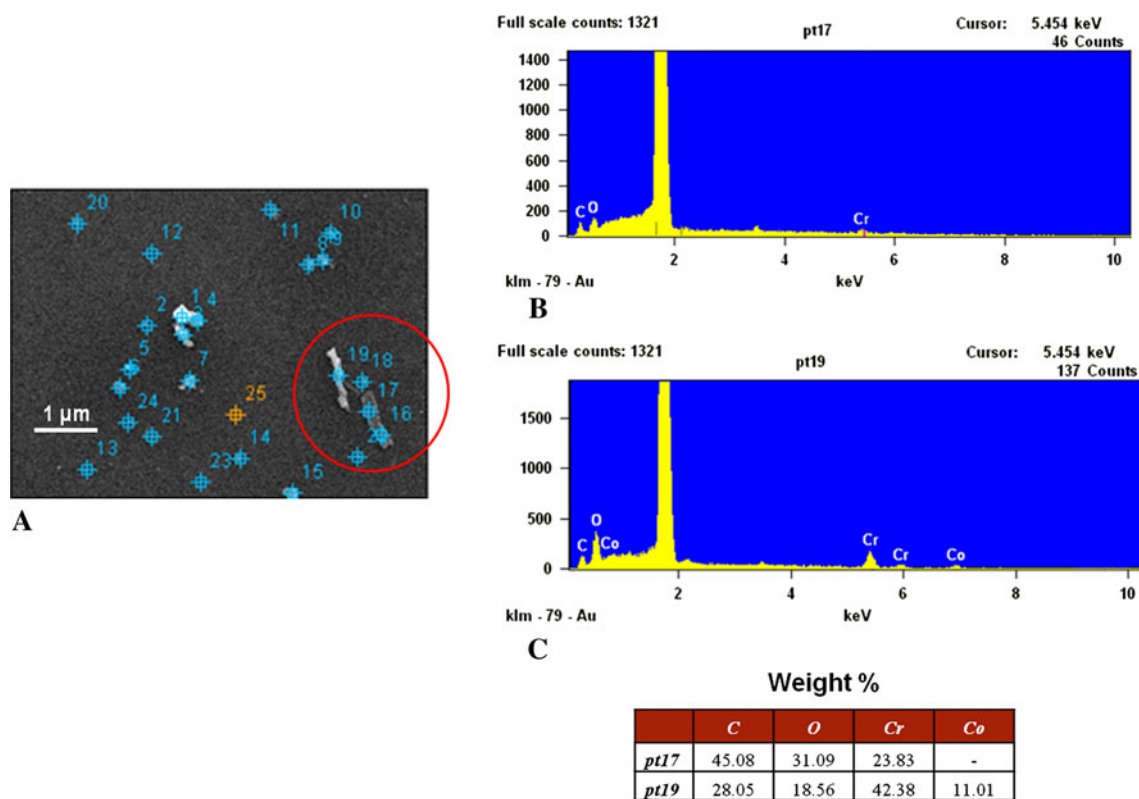


Fig. 11A–C Images show the chemical characterization of particles on a wafer. **(A)** On a low-resolution image of the analyzed wafer area acquired via EDS software, particles were automatically identified (marked on the image) and numbered; some particles cannot be distinguished from the marks because of the low resolution and small

particle dimension. Spectra are shown from the particles in the circle in **(A)**, specifically from **(B)** Point 17, which is a Co-rich particle and dark, and **(C)** Point 19, which is from a particle mainly composed of CrOx and bright.

simple dimensional measurements. We defined the shape of the particles by several parameters extracted via image analysis. This minimized operator sensitivity, providing an objective measurement that could be correlated with other parameters (Fig. 10).

A reliable morphologic characterization allows for establishing correlations between particles and wear mechanisms. Tribologic properties of materials strongly affect characteristics of wear particles. Conversely, particle characteristics can often provide information regarding not only the magnitude of wear but also the types of underlying wear mechanisms. Particles retrieved from MOM hip implants are nanometer in size, round or oval in shape, and mostly CrOx. This is consistent with normal conditions of use and continuous generation and removal of the protective layer of a metal surface, indicating mild abrasive wear. Implant surfaces showed light scratches and polishing with low values of wear ($< 1 \text{ mm}^3/\text{million cycles}$). However, particles from MOM lumbar spine implants ($> 10 \text{ mm}^3/\text{million cycles}$) had larger average d_{max} and more irregular, Co-rich particles, indicating severe abrasion. Analysis of the surface of the implants showed severe wear and signs

of impingement [29]. Several authors suggest microstructural changes at and below the surface are responsible for generating nanometer-sized wear debris with MOM implants [5, 42]. Such substructures with amorphous and crystalline regions are characterized as containing chromium, oxygen, and carbon (Fig. 11). These particles may be the result of mechanical mixing and tribochemical reactions at the alloy surface [42].

In summary, the MC-SWD protocol provided an integrated experimental platform for isolation and characterization of metal and ceramic wear debris. It is applicable to any hard-on-hard bearing couple producing low wear because of its capacity to concentrate particles without aggregation. In addition, it yielded uniform, two-dimensional particle displays on a featureless surface without filter pores for high-resolution automated chemical and morphologic analysis and high particle recovery. The protocol allowed distinguishing particles of interest from environmental contaminants, highlighting the importance of particle separation and particle-specific analysis by composition and morphology. Finally, because it shares a protease digestion step and early material-dependent

particle separation with the polyethylene SWD protocol, the two protocols can be used simultaneously on a single sample containing multiple materials (eg, polyethylene and CoCr).

References

- Anissian HL, Stark A, Gustafson A, Good V, Clarke IC. Metal-on-metal bearing in hip prosthesis generates 100-fold less wear debris than metal-on-polyethylene. *Acta Orthop Scand*. 1999;70:578–582.
- ASTM International. ASTM F1877-05. *Standard Practice for Characterization of Particles*: West Conshohocken, PA: ASTM International; 2005.
- Billi F, Benya P, Ebramzadeh E, Campbell P, Chan F, McKellop HA. Metal wear particles: what we know, what we do not know, and why. *SAS J*. 2009;3:133–142.
- Brown C, Williams S, Tipper JL, Fisher J, Ingham E. Characterisation of wear particles produced by metal on metal and ceramic on metal hip prostheses under standard and microseparation simulation. *J Mater Sci Mater Med*. 2007;18:819–827.
- Buscher R, Tager G, Dudzinski W, Gleising B, Wimmer MA, Fischer A. Subsurface microstructure of metal-on-metal hip joints and its relationship to wear particle generation. *J Biomed Mater Res B Appl Biomater*. 2005;72:206–214.
- Campbell P, Beaulé PE, Ebramzadeh E, LeDuff M, De Smet K, Lu Z, Amstutz HC. The John Charnley Award. A study of implant failure in metal-on-metal surface arthroplasties. *Clin Orthop Relat Res*. 2006;453:35–46.
- Campbell P, Ebramzadeh E, Nelson S, Takamura K, De Smet K, Amstutz H. Are adverse periprosthetic tissue reactions caused by high metal-on-metal wear or hypersensitivity? *Clin Orthop Relat Res*. 2010;468:2321–2327.
- Campbell P, McKellop H, Alim R, Mirra J, Nutt S, Dorr LD, Amstutz HC. Metal-on-metal hip replacements: wear performance and cellular response to wear particles. In: Disegi JA, Kennedy RL, Pilliar R, eds. *Cobalt Base Alloys for Biomedical Applications*. STP 1365. West Conshohocken, PA: ASTM International; 1999:193–209.
- Campbell P, Shen FW, McKellop H. Biologic and tribologic considerations of alternative bearing surfaces. *Clin Orthop Relat Res*. 2004;418:98–111.
- Catelas I, Bobyn JD, Medley JB, Krygier JJ, Zukor DJ, Petit A, Huk OL. Effects of digestion protocols on the isolation and characterization of metal-metal wear particles. I. Analysis of particle size and shape. *J Biomed Mater Res*. 2001;55:320–329.
- Catelas I, Bobyn JD, Medley JJ, Zukor DJ, Petit A, Huk OL. Effects of digestion protocols on the isolation and characterization of metal-metal wear particles. II. Analysis of ion release and particle composition. *J Biomed Mater Res*. 2001;55:330–337.
- Catelas I, Medley JB, Campbell PA, Huk OL, Bobyn JD. Comparison of in vitro with in vivo characteristics of wear particles from metal-metal hip implants. *J Biomed Mater Res*. 2004;70:167–178.
- Chan FW, Bobyn JD, Medley JB, Krygier JJ, Tanzer M. The Otto Aufranc Award. Wear and lubrication of metal-on-metal hip implants. *Clin Orthop Relat Res*. 1999;369:10–24.
- De Haan R, Campbell PA, Su EP, De Smet KA. Revision of metal-on-metal resurfacing arthroplasty of the hip: the influence of malposition of the components. *J Bone Joint Surg Br*. 2008;90:1158–1163.
- Doom PF, Campbell PA, Amstutz HC. Metal versus polyethylene wear particles in total hip replacements: a review. *Clin Orthop Relat Res*. 1996;329(Suppl):S206–S216.
- Doom PF, Campbell PA, Worrall J, Benya PD, McKellop HA, Amstutz HC. Metal wear particle characterization from metal on metal total hip replacements: transmission electron microscopy study of periprosthetic tissues and isolated particles. *J Biomed Mater Res*. 1998;42:103–111.
- Doom PF, Mirra JM, Campbell PA, Amstutz HC. Tissue reaction to metal on metal total hip prostheses. *Clin Orthop Relat Res*. 1996;329(Suppl):S187–S205.
- Dunstan E, Sanghrajka AP, Tilley S, Unwin P, Blunn G, Cannon SR, Briggs TW. Metal ion levels after metal-on-metal proximal femoral replacements: a 30-year follow-up. *J Bone Joint Surg Br*. 2005;87:628–631.
- Esposito C, Walter WL, Campbell P, Roques A. Squeaking in metal-on-metal hip resurfacing arthroplasties. *Clin Orthop Relat Res*. 2010;468:2333–2339.
- Firkins PJ, Tipper JL, Saadatzadeh MR, Ingham E, Stone MH, Farrar R, Fisher J. Quantitative analysis of wear and wear debris from metal-on-metal hip prostheses tested in a physiological hip joint simulator. *Biomed Mater Eng*. 2001;11:143–157.
- Fisher J, Hu XQ, Tipper JL, Stewart TD, Williams S, Stone MH, Davies C, Hatto P, Bolton J, Riley M, Hardaker C, Isaac GH, Berry G, Ingham E. An in vitro study of the reduction in wear of metal-on-metal hip prostheses using surface-engineered femoral heads. *Proc Inst Mech Eng H*. 2002;216:219–230.
- Granchi D, Savarino L, Ciapetti G, Cenni E, Rotini R, Mieti M, Baldini N, Giunti A. Immunological changes in patients with primary osteoarthritis of the hip after total joint replacement. *J Bone Joint Surg Br*. 2003;85:758–764.
- Hart AJ, Sabah S, Henckel J, Lewis A, Cobb J, Sampson B, Mitchell A, Skinner JA. The painful metal-on-metal hip resurfacing. *J Bone Joint Surg Br*. 2009;91:738–744.
- Hirakawa K, Bauer TW, Stulberg BN, Wilde AH, Secic M. Characterization and comparison of wear debris from failed total hip implants of different types. *J Bone Joint Surg Am*. 1996;78:1235–1243.
- International Organization for Standardization. ISO 18192-1:2008. *Implants for Surgery: Wear of Total Intervertebral Spinal Disc Prostheses. Part 1: Loading and Displacement Parameters for Wear Testing and Corresponding Environmental Conditions for Test*. Washington, DC: International Organization for Standardization; 2008.
- Jacobs JJ, Hallab NJ. Loosening and osteolysis associated with metal-on-metal bearings: a local effect of metal hypersensitivity? *J Bone Joint Surg Am*. 2006;88:1171–1172.
- Keegan GM, Learmonth ID, Case CP. Orthopaedic metals and their potential toxicity in the arthroplasty patient: a review of current knowledge and future strategies. *J Bone Joint Surg Br*. 2007;89:567–573.
- Korovessis P, Petsinis G, Repanti M, Repantis T. Metallosis after contemporary metal-on-metal total hip arthroplasty: five to nine-year follow-up. *J Bone Joint Surg Am*. 2006;88:1183–1191.
- Lee JL, Billi F, Sangiorgio SN, McGarry W, Krueger DJ, Miller PT, McKellop H, Ebramzadeh E. Wear of an experimental metal-on-metal artificial disc for the lumbar spine. *Spine (Phila Pa 1976)*. 2008;33:597–606.
- Leslie I, Williams S, Brown C, Isaac G, Jin Z, Ingham E, Fisher J. Effect of bearing size on the long-term wear, wear debris, and ion levels of large diameter metal-on-metal hip replacements—an in vitro study. *J Biomed Mater Res B Appl Biomater*. 2008;87:163–172.
- Leslie IJ, Williams S, Brown C, Anderson J, Isaac G, Hatto P, Ingham E, Fisher J. Surface engineering: a low wearing solution for metal-on-metal hip surface replacements. *J Biomed Mater Res B Appl Biomater*. 2009;90:558–565.

32. McKellop H, Shen FW, Lu B, Campbell P, Salovey R. Effect of sterilization method and other modifications on the wear resistance of acetabular cups made of ultra-high molecular weight polyethylene: a hip-simulator study. *J Bone Joint Surg Am.* 2000;82:1708–1725.
33. Pandit H, Glyn-Jones S, McLardy-Smith P, Gundle R, Whitwell D, Gibbons CL, Ostlere S, Athanasou N, Gill HS, Murray DW. Pseudotumours associated with metal-on-metal hip resurfacings. *J Bone Joint Surg Br.* 2008;90:847–851.
34. Park YS, Moon YW, Lim SJ, Yang JM, Ahn G, Choi YL. Early osteolysis following second-generation metal-on-metal hip replacement. *J Bone Joint Surg Am.* 2005;87:1515–1521
35. Paul JP. Force actions transmitted by joints in the human body. *Proc R Soc Lond B Biol Sci.* 1976;192:163–172.
36. Savio JA 3rd, Overcamp LM, Black J. Size and shape of bio-material wear debris. *Clin Mater.* 1994;15:101–147.
37. Schmalzried TP. Metal-metal bearing surfaces in hip arthroplasty. *Orthopaedics.* 2009;32. pii: orthosupersite.com/view.asp?rID = 42831. doi: [10.3928/01477447-20090728-06](https://doi.org/10.3928/01477447-20090728-06).
38. Schmiedberg SK, Chang DH, Frondoza CG, Valdevit AD, Kostuik JP. Isolation and characterization of metallic wear debris from a dynamic intervertebral disc prosthesis. *J Biomed Mater Res.* 1994;28:1277–1288.
39. Sieber HP, Rieker CB, Kottig P. Analysis of 118 second-generation metal-on-metal retrieved hip implants. *J Bone Joint Surg Br.* 1999;81:46–50.
40. Thomas P, Braathen LR, Dörig M, Auböck J, Nestle F, Werfel T, Willert HG. Increased metal allergy in patients with failed metal-on-metal hip arthroplasty and peri-implant T-lymphocytic inflammation. *Allergy.* 2009;64:1157–1165.
41. Tipper JL, Firkins PJ, Ingham E, Fisher J, Stone MH, Farrar R. Quantitative analysis of the wear and wear debris from low and high carbon content cobalt chrome alloys used in metal on metal total hip replacements. *J Mater Sci Mater Med.* 1999;10:353–362.
42. Wimmer MA, Fischer A, Buscher R, Pourzal R, Sprecher C, Hauert R, Jacobs JJ. Wear mechanisms in metal-on-metal bearings: the importance of tribochemical reaction layers. *J Orthop Res.* 2009;28:436–443.